

Jet driven motions in the Narrow Line Region of NGC 1068 ¹

D.J. Axon^{2,3}, A. Marconi^{4,5}

*Space Telescope Science Institute
3700 San Martin Drive
Baltimore, MD 21218*

A. Capetti

*Osservatorio Astronomico di Torino
Strada Osservatorio 25
40025, Pino Torinese, Italy*

F.D. Macchetto², E. Schreier

Space Telescope Science Institute

A. Robinson

*Division of Physics and Astronomy,
Department of Physical Sciences,
University of Hertfordshire,
College Lane, Hatfield, Herts AL10 9AB, UK*

ABSTRACT

We have obtained HST FOC f/48 long-slit spectroscopy of the inner 4 arcseconds of the Narrow Line Region of NGC 1068 between 3500-5400Å with a spectral resolution of 1.78Å/pixel. At a spatial scale of 0".0287 per pixel these data provide an order of magnitude improvement in resolution over previous ground based spectra and allow us to trace the interaction between the radio jet and the gas in the NLR. Our results show that, within $\pm 0".5$ of the radio-jet the emission lines are kinematically disturbed

¹Based on observations with the NASA/ESA Hubble Space Telescope, obtained at the Space Telescope Science Institute, which is operated by AURA, Inc., under NASA contract NAS 5-26555 and by STScI grant GO-3594.01-91A

²Affiliated to the Astrophysics Division, Space Science Department, ESA

³On leave from the University of Manchester

⁴Dipartimento di Astronomia e Scienza dello Spazio, Università di Firenze, Largo E. Fermi 5, I-50125, Italy

⁵Osservatorio Astrofisico di Arcetri, Largo E. Fermi 5, I-50125, Italy

and split into two components whose velocity separation is 1500 km s^{-1} . The filaments associated with the radio lobe also show a redshifted kinematic disturbance of the order of 300 km s^{-1} which probably is a consequence of the expansion of the radio plasma.

Furthermore, the material enveloping the radio-jet is in a much higher ionization state than that of the surrounding NLR gas. The highest excitation is coincident with the jet axis where emission in the coronal line of $[\text{FeVII}] \lambda 3769 \text{ \AA}$ is detected and the $\text{He II} \lambda 4686 \text{ \AA}$ is strong but where $[\text{OII}] \lambda 3727 \text{ \AA}$ is depressed. This large localized increase in ionization on the jet axis is accompanied by the presence of an excess continuum. Because the electron density is substantially larger in the jet compared to the surrounding NLR, these results can only be explained if there is a more intense ionizing continuum associated with the jet. This can be accomplished in a variety of ways which include an intrinsically anisotropic nuclear radiation field, a reduced gas covering factor or the presence of a local ionization source.

The morphology, kinematics and, possibly, the ionization structure of the NLR in the vicinity of the jet of NGC 1068 are a direct consequence of the interaction with the radio outflow.

Subject headings: Galaxies - individual (NGC1068); Galaxies - Seyfert; Galaxies - active

1. Introduction

Extensive HST emission line imagery of the Narrow Line Regions (NLR) of Seyfert galaxies with linear radio sources has shown that the morphology of the NLR is directly related to that of the radio emission. Seyfert galaxies with a lobe-like radio morphology (e.g. Mrk 573, Mrk 78, NGC 3393, IRAS 0421+045 and IRAS 1105-035) have bow-shock shaped emission line regions (Bower et al. 1994, Axon et al. 1996, Capetti et al. 1996), while those with a jet-like radio structure (e.g. Mrk 3, Mrk 348, Mrk 6, Mrk1066) have jet-like emission line structures (Bower et al. 1995, Capetti et al. 1995a, Capetti et al. 1995b). These results have provided compelling evidence for strong dynamical interactions between the emission line gas and radio-emitting ejecta on scales of ≤ 1 kpc.

The physical foundation of this picture was first developed by Taylor, Dyson and Axon (1992) who constructed fast bow shock models for the interaction between radio ejecta and the ISM which included the effects of photo-ionization from the nucleus. Dopita and Sutherland (Dopita & Sutherland 1996a, Dopita & Sutherland 1996b) have emphasized that the hot shocked gas could itself make an important local contribution to the ionizing continuum (becoming what they termed an *auto-ionizing* shock).

NGC 1068 is one of the closest Seyfert galaxies and it harbours a bright radio source, with a prominent radio-jet (Muxlow et al. 1996) terminating in an extended radio-lobe (Wilson & Ulvestad 1983). Ground-based kinematic studies of the NLR have been carried out previously by a number of authors (Alloin et al. 1983, Baldwin et al. 1987, Meaburn and Pedlar 1986, Cecil, Bland & Tully 1990, Unger et al. 1992, Arribas et al. 1996) in [OIII] $\lambda 5007$. In particular two broad components straddling a narrow central component in the NE radio lobe were identified. The narrow component appears to follow the expected rotation curve of the galaxy and is

emitted by undisturbed gas in the disk. At larger radii this triple structure disappears.

The complexity of the velocity field observed in the inner region is almost certainly due to the spatial confusion caused by projection and seeing effects which mixes kinematic components from different regions along the line of sight. In particular the velocity structure created by the expansion of the hot gas associated with the lobe is projected onto the region interacting with the jet which can be spatially resolved only with HST. In order to obtain a more detailed picture of the relationship between the velocity field and the ionization conditions in the NLR gas and the interaction of the gas with the radio jet we have therefore obtained new long-slit spectroscopic observations with the Faint Object Camera f/48 spectrograph on board the HST. Our results allow us to resolve the spatial confusion and provide evidence that shocks created by the jet play a key role in forming and, possibly, ionizing the NLR of NGC 1068. Throughout this paper we will adopt a distance to NGC 1068 of 14.4 Mpc (Tully 1988) where $1''$ corresponds to 72 pc.

2. Observations and Data Reduction

The Narrow Line Region of NGC 1068 was observed using the FOC f/48 long-slit spectrograph on October 18th, 1996 at resolutions of 1.78\AA and $0''.0287$ per pixel along the dispersion and slit directions, respectively. The F305LP filter was used to isolate the first order spectrum which covers the 3650–5470 \AA region and therefore includes the [O II] $\lambda 3727$, H $\beta\lambda 4861$ and [O III] $\lambda\lambda 4959, 5007$ \AA emission lines. The slit, $0''.063 \times 13''.5$ in size, was placed at a position angle of 83° and spectra with exposure times of 627 seconds were taken in the 1024x512 non-zoomed mode at 6 locations separated by $1''$. Unfortunately, due to a guide star re-acquisition failure, only 3 of the slit locations yielded usable spectra which we identify as POS1, POS2 and POS3 respectively.

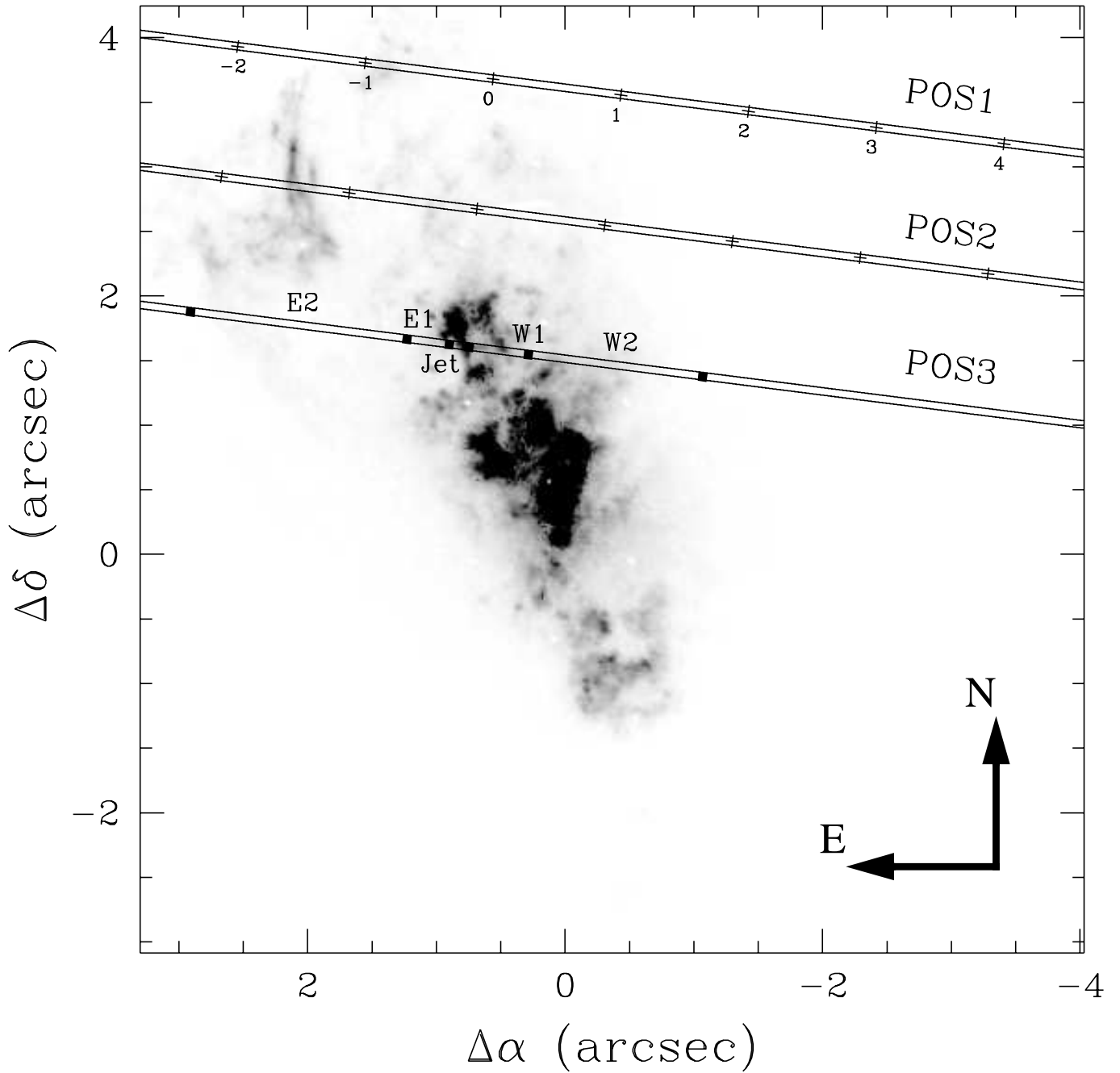


Fig. 1.— The slit positions used in our study overlaid on a gray scale map of the [OIII] image of Macchetto et al. 1994. The origin of the spatial axis on the borders of the image is centered on the position of the hidden nucleus (Capetti et al. 1995c). The spatial coordinates used along the slit are marked as crosses at POS1 and POS2. The zero point of this axis lies on cloud G in POS3. The filaments associated with the radio lobe intersect the slit at POS2 at location -1.5 arcseconds and POS1 at -1 arcseconds. The filled squares at POS3 indicate the limits of the contiguous regions where we extracted the spectra shown in Fig. 3.

The data reduction follows the procedure described in detail by Macchetto et al. 1997. Flux calibration was performed using the observations of the spectrophotometric standard star LDS749b.

To accurately determine the location of the slits we compared the surface brightness profile derived from the FOC, f/96, F501N HST image of Macchetto et al. 1994 with that measured from the spectra at the three slit positions. The best match is displayed in Fig. 1 and is accurate to within half a slit width ($\simeq 0''.03$).

The slit locations POS1 and POS2 cut across the emission line filament system associated with the Northern radio lobe (Capetti, Axon, & Macchetto 1997). While the slit at POS3 (see Fig. 1) traverses cloud G (Evans et al. 1991) and the parallel feature to the West which form a funnel-like structure where the jet meets the radio lobe (see Gallimore et al. 1996).

3. Results

The velocities derived from the [O III] and [O II] lines by fitting gaussian line profiles are plotted in Fig. 2. Around the jet axis, at POS3 (Fig. 2b), the lines are split into two velocity systems separated by $\sim 1500 \text{ km s}^{-1}$. Outside this region the gas motions are quiescent but with a gradient of $+500 \text{ km s}^{-1}$ from West to East. Notice that the velocity splitting is not symmetric about the systemic velocity, but is much larger on the blue-shifted side. The blueshifted component is also substantially brighter and has a larger velocity dispersion than the redshifted component. At POS2 (Fig. 2a) the velocity field is relatively flat, except at the filaments at slit coordinates $\sim -1'' - -2''$, where there is a large redshifted velocity perturbation of amplitude $\sim 300 \text{ km s}^{-1}$, at a similar radial velocity to that of the redshifted component of the split line region in POS3. POS1 (Fig. 2a) shows a similar pattern in velocity, but with a reduced amplitude in the perturbed region.

Turning to the emission line strengths, in Fig. 3 we show plots of representative spectra from the five regions identified in Fig. 1. On the jet axis (labeled as “Jet”) the gas is highly ionized; [Fe VII] $\lambda 3759\text{\AA}$ and [Ar IV] are clearly visible and the He II $\lambda 4686$ is as high as 0.7 the strength of H β , while the [O II] emission appears to be depressed. This increase in excitation is accompanied by the presence of an excess local continuum, as shown in Fig. 4.

Outside the jet the excitation conditions are much lower, with [O II] being relatively stronger, particularly to the E as shown in Fig. 4. The variation of the [O III]/[O II] ratio along the slit, plotted in Fig. 5, shows that there is a factor $\simeq 5$ difference between the ratio on the jet axis and outside. The electron temperature measured from the [O III] $\lambda\lambda 4363/5007$ ratio give $T_e = (1.15 \pm 0.15) \times 10^4 \text{ K}$. A lower limit for the electron density can be obtained from the [Ar IV] $\lambda\lambda 4710/4740$ ratio and yields $N_e \geq 10^{4.5} \text{ cm}^{-3}$. At similar distances from the nucleus, but off the jet, ground based density measurements from [S II] $\lambda\lambda 6716,6731$ ratio, obtained from our unpublished spectroscopy, indicate electron densities of a few 100 cm^{-3} . Thus the increase in excitation on the jet occurs despite an increase in density.

4. Discussion

The morphological connection between the optical and radio emission in the region of the jet has been discussed in detail by Gallimore et al. (1996) and by Capetti, Macchetto and Lattanzi (1997). They showed that there is a clear anti-correlation between radio and optical emission, with the brightest line emitting knots surrounding the radio-jet. In the jet-cloud interaction picture, the radio jet clears a channel through the cool ISM, leaving hot ionized gas in its wake and the line emission is highly enhanced along the edges of the radio-jet where the gas is compressed.

The overall velocity structure and ionization

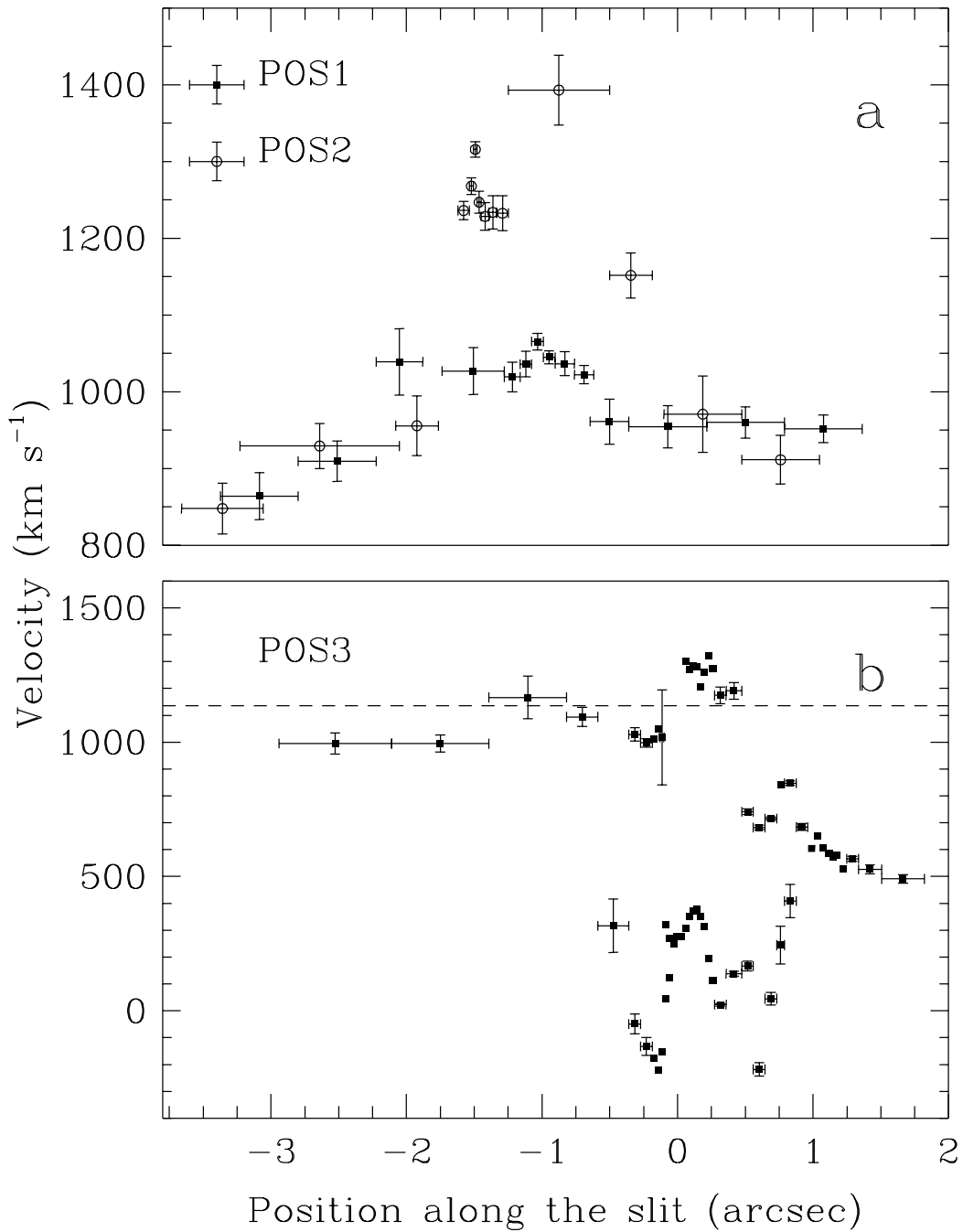


Fig. 2.— Velocity fields measured at the three slit positions. Lower panel: Around the jet axis, at POS3, the gas is strongly kinematically perturbed and shows split lines with components separated by ~ 1500 km s^{-1} . The dashed line marks the systemic velocity of NGC 1068 (Baan & Haschick 1983). Upper panel: at POS2 and POS1 there are also large velocity perturbation at the location of the emission line filaments.

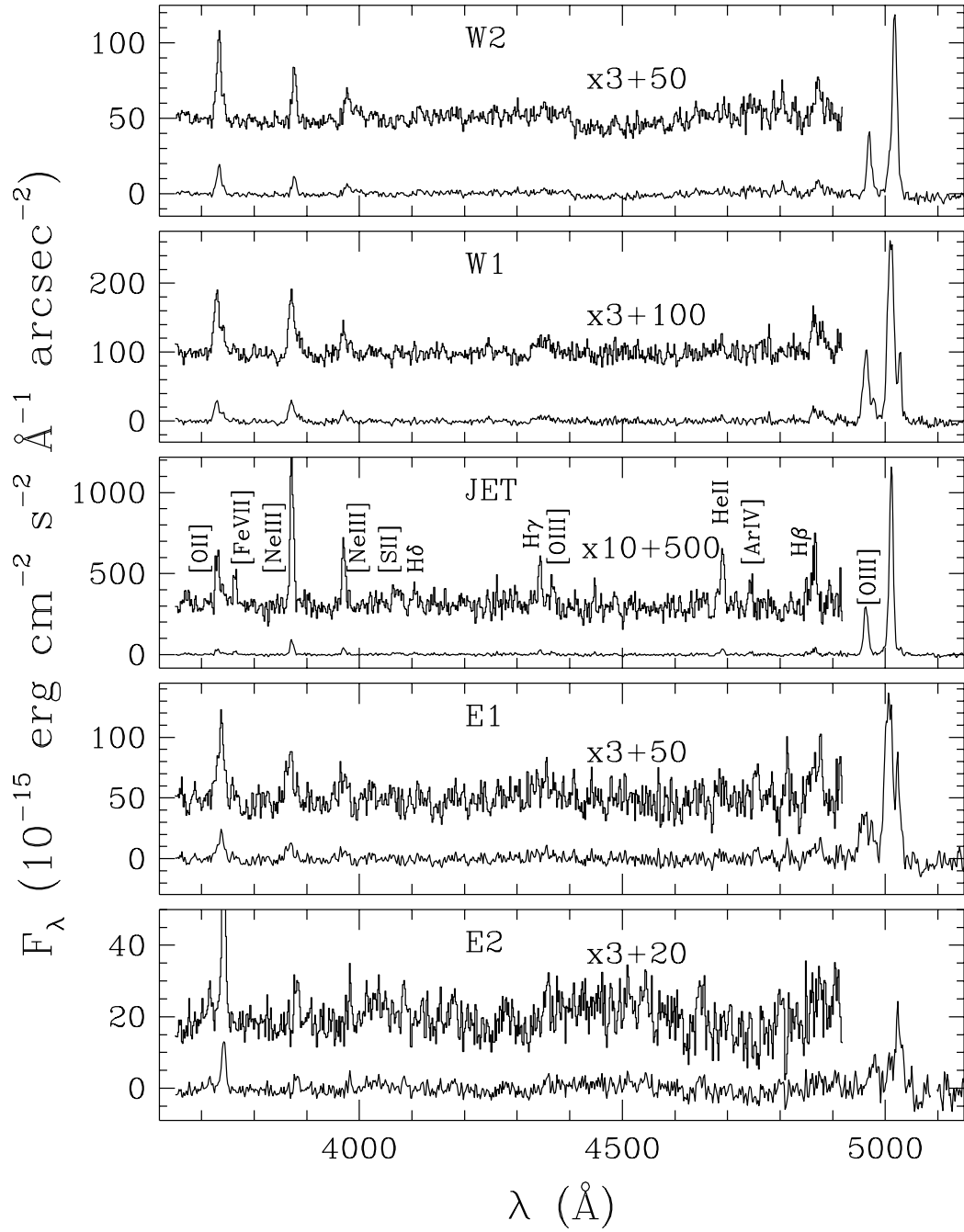


Fig. 3.— Spectra extracted at the positions indicated in Fig. 1. The spectrum extracted in a $0''.14 \times 0''.063$ aperture around cloud G, labeled "Jet", shows the high excitation gas on the jet with [Fe VII], [Ar IV] and He II emission lines.

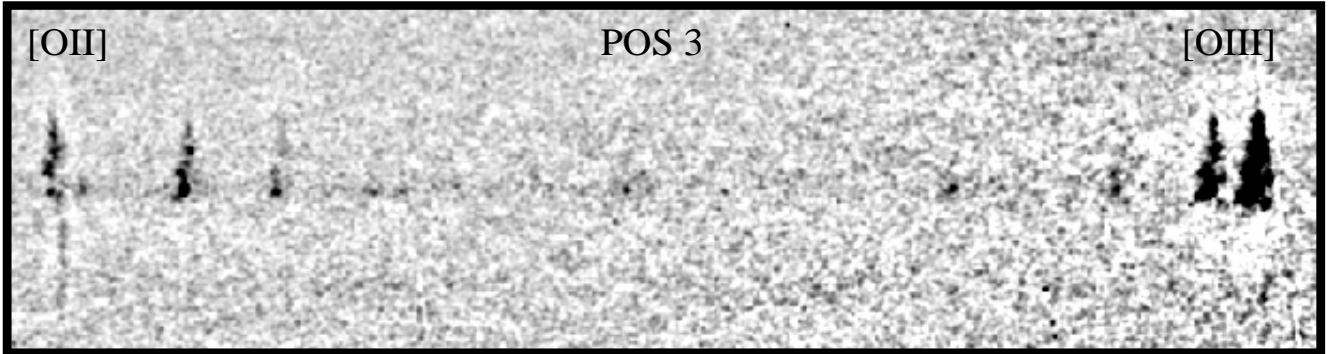


Fig. 4.— Grey scale image of the spectrum at POS3 showing the excess continuum associated with the radio jet.

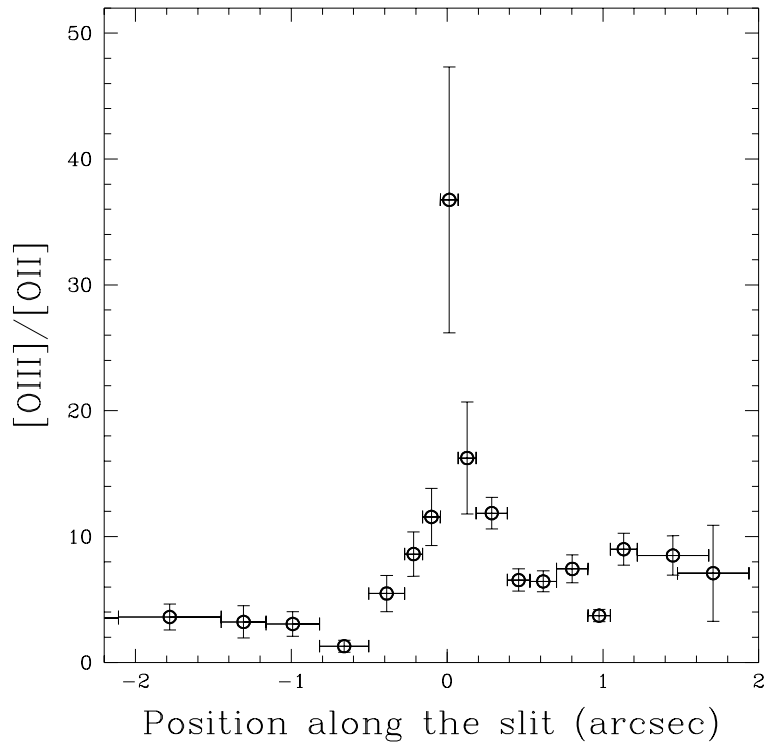


Fig. 5.— A plot of the $[OIII]/[OII]$ ratio as a function of position along the slit at POS 3. The ratio reaches a maximum on the jet axis where it is ~ 5 times larger than that in the surrounding regions.

conditions of the gas associated with the jet of NGC1068 can be understood in terms of this picture of an expanding and cooling cocoon around the jet which creates very fast shocks with at least $V \simeq 700 \text{ km s}^{-1}$ (even when mass-loading of the expanding cocoon is taken into account).

The viewing angle is such that to the NE the lobe is projected on to the disk of NGC1068, so that the jet is seen emerging towards us out of the disk. The situation is very similar to that seen previously on the jet of 3C120 (Axon et al. 1989), even down to the clumpy structure of the gas, which almost certainly arises because of the onset of instabilities caused by the mixing of hot and cold material. This morphology is again readily understood if it is due to the interaction between the jet and the surrounding medium. A viable explanation for the observed asymmetry of the velocity splitting is that it is due to density stratification of the disk, that is the expanding hot bubble is able to expand more rapidly along the density gradient away from the disk plane, than towards it. Further weight to this argument is provided by the systematic blue-shift of coronal lines with respect to the lower excitation lines (Marconi et al. 1996). This implies that the coronal lines comes from a different kinematic component which we would ascribe to the hot cooling gas in the cocoon.

The spectral diagnostics obtained from our long-slit spectra indicate that the kinematically disturbed line-emitting gas associated with the radio jet has both a higher density and a higher excitation level than the surrounding NLR. A similar result, based on narrow band imaging, has been reported recently by Capetti, Axon, & Macchetto 1997. The density enhancement is a factor > 100 if the ground-based measurements of the $[\text{SII}]\lambda\lambda 6716, 6731$ ratio can be taken as typical of the regions extending away from the jet axis. On the other hand, the variations in the $[\text{OIII}]\lambda 5007/[\text{OII}]\lambda 3727$ ratio along the POS 3 slit imply a factor 5 enhancement in the ionization parameter (U) across the jet axis (since this ratio

is approximately proportional to U ; Penston et al 1989). The enhancements in both density *and* ionization parameter imply that the local ionizing radiation is a factor ~ 500 higher at the location of the jet in POS 3, than it is elsewhere. The exceptionally strong $[\text{Fe VII}]$ and HeII lines suggest that matter-bounded clouds might contribute significantly to the line emission near the jet. In this case, we will be overestimating the jump in U since low ionization lines such as $[\text{OII}]$ are strongly suppressed in such clouds. Nevertheless, this is unlikely to explain the whole of the inferred increase in the ionizing flux. Either a local ionization source is present which dominates the AGN radiation field near the jet axis, or the AGN radiation field is itself highly anisotropic.

The most important local ionization source is likely to be ionizing radiation (free-free and high ionization line emission) from gas heated and ionized in fast shocks driven by the radio jet (Binette, Dopita & Tuohy, 1985; Sutherland, Bicknell & Dopita 1993; Dopita & Sutherland 1996a,b). The strong $[\text{Fe VII}]$ emission and the excess continuum observed on the jet axis may be a clue that the coronal gas expected in this picture is indeed present. Alternatively, the on-axis increase in the ionizing flux could be attributed to intrinsic anisotropy of the nuclear continuum. In this case, the size of the enhancement in flux, and the fact that it is highly localized, require a continuum beaming factor comparable with Doppler boosting in a moderately relativistic jet ($\gamma = \text{a few}$). This idea can be ruled out because the region we have studied occurs after a significant bend of the jet and therefore one would expect to see higher excitation along the original jet direction, which is not observed (cf. Capetti, Axon, & Macchetto 1997).

Perhaps a more likely explanation is that the continuum anisotropy is largely produced by azimuthal variations in the optical depth to ionizing photons. In this picture, the radio jet sweeps out a channel as it passes through the NLR with the result that ionizing radiation from the cen-

tral source suffers much less attenuation along its axis than in other directions.

Our results on POS1 and POS2 can also be interpreted in terms of the interaction between the radio plasma and the ambient gas, but in this case it is the expanding lobe material which is driving the motion. From our spectroscopic data we can say little on the ionization conditions of these filaments because only the [O III] lines are detected.

5. Conclusions

We have presented new HST FOC f/48 long-slit spectra of the central 4 arcseconds of the NLR of NGC 1068. At a spatial scale of $0''.0287$ per pixel these data provide an order of magnitude improvement in resolution over previous ground based spectra and allow us to trace the interaction between the radio jet and the gas in the NLR. Our results show that, within $\pm 0''.5$ of the radio-jet the emission lines are split into two components whose velocity separation is ~ 1500 km s $^{-1}$ and are clearly the result of the interaction between the radio jet and the ambient NLR material. The filaments associated with the radio lobe also show a redshifted kinematic disturbance of the order of 300 km s $^{-1}$ which probably is a consequence of the expansion of the radio plasma.

Our results show that the highest excitation gas is physically related to the location of the jet and is accompanied by an excess continuum providing additional evidence for the interaction model.

The morphology, kinematics and, possibly, the ionization structure of the NLR in the vicinity of the jet of NGC 1068 are a direct consequence of the interaction with the radio outflow.

A.M. acknowledges partial support through GO grant G005.44800 from Space Telescope Science Institute, which is operated by the Association of Universities for Research in Astronomy,

Inc., under NASA contract NAS 5-26555. A.C. thanks the STScI visitor program for providing financial support during the course of this work. A.R. is supported by a Royal Society Fellowship. We thank E. Oliva for kindly providing his compilation of atomic parameters and his code to derive line emissivities.

REFERENCES

- Alloin, D., Pelat, D, Boksenberg, A, & Sargent, W., 1983, ApJ, 275, 493.
- Arribas, S., Mediavilla, E., Garcia-Lorenzo, B., 1996, ApJ 463, 509
- Axon, D. J., Unger, S. W., Pedlar, A., Meurs, E. J. A, Whittle, D. M. & Ward, M. J., 1989, Nature, 341, 631-633.
- Baan W.A. and Haschick A.D., 1983, AJ, 88, 1088
- Axon, D. J., Capetti, A., Macchetto, F., Sparks, W. B. & Boksenberg, A. 1996, In Science with the Hubble Space Telescope- II, ed P. Benvenuti, F.D. Macchetto & E. J. Schreier, 214-218.
- Baldwin, J., Wilson, A.S., & Whittle, M., 1987, ApJ, 319, 84.
- Binette, L., Dopita, M.A., Tuohy, I.R., 1985, ApJ, 297, 476
- Bower, G., Wilson, A.S., Mulchaey, J., Miley, G.K., Heckman, T.M., and Krolik, J.H., 1994, AJ, 107, 1686.
- Bower, G., Wilson, A.S., Morse, J.A., Gelderman, R., Whittle, M., and Mulchaey, J., 1995, ApJ, 454, 106.
- Capetti, A., Macchetto, F.D., Axon, D.J., Sparks, W.B., and Boksenberg, A. 1995a, ApJ, 448, 600.
- Capetti, A., Axon, D.J., Kukula, M., Macchetto F.D., Pedlar, A., Sparks, W.B., and Boksenberg, A. 1995b, ApJ, 454, 85.

- Capetti, A., Macchetto, F.D., Axon, D.J., Sparks, W.B., and Boksenberg, A. 1995c, ApJ, 452, L87.
- Capetti, A., Axon, D. J., Macchetto F. D., Sparks, W. B., and Boksenberg, A. 1996, ApJ, 469, 554.
- Capetti, A., Axon, D. J., & Macchetto F. D. 1997, ApJ, 487, 560
- Capetti A., Macchetto F.D., Lattanzi M.G., 1997, ApJ, 476, 67
- Cecil, G, Bland, J. & Tully, R., 1990, ApJ, 355, 70.
- Dopita, M.A. & Sutherland, R.S. 1996a, ApJ, 455, 468.
- Dopita, M.A. & Sutherland, R.S. 1996b, ApJS, 102, 161.
- Evans, I. N., Ford, H. C., Kinney, A. L., Antonucci, R. R. J., Armus, L., and Caganoff, S. 1991, ApJ 369, 27
- Gallimore, J.F., Baum, S.A., O’Dea, C.P., and Pedlar, A., 1996, ApJ, 458, 136.
- Macchetto, F. D., Capetti, A., Sparks, W. B., Axon, D. J., and Boksenberg, A. 1994, ApJ, 435, 15.
- Macchetto, F. D., Marconi, A., Axon, D. J., Capetti, A., Sparks, W. B., and Crane, P. 1997, ApJ, 489, 579
- Marconi A., van der Werf P.P., Moorwood A.F.M., and Oliva E., A&A, 1996, 315, 335
- Meaburn, J. & Pedlar, A., 1986, Astron. & Astrophys., 159, 336.
- Muxlow, T. W. B., Pedlar, A., Holloway, A. J., Gallimore, J. F., and Antonucci, R. R. J. 1996, MNRAS, 278, 854.
- Sutherland, R.S., Bicknell, G.V., and Dopita, M.A., 1993, ApJ, 414, 506.
- Taylor, D., Dyson, J., and Axon, D. J. 1992, MNRAS, 255, 35.
- Tully, R.B., 1988, Nearby Galaxies catalog, Cambridge University Press
- Unger, S.W., Lewis, J.R., Pedlar, A., and Axon, D.J. 1992, MNRAS, 258, 371.
- Wilson, A.S., & Ulvestad, J.S., 1983, ApJ, 275, 8.